POLITECNICO DI TORINO
Repository ISTITUZIONALE

Development of a virtual methodology based on physical and data-driven models to optimize engine calibration

Publisher copyright

(Article begins on next page)

29 November 2022
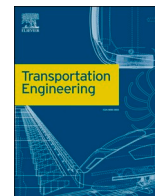
Full Length Article

Development of a virtual methodology based on physical and data-driven models to optimize engine calibration

G. Boccardo [a], A. Piano [b,*], A. Zanelli [a], M. Babbi [b], L. Cambriglia [a], S. Mosca [c], F. Millo [b]

[a] POWERTECH Engineering S.r.l., Turin, ITALY
[b] Energy Department, Politecnico di Torino, Turin, ITALY
[c] Modelway S.r.l., Turin, ITALY

A B S T R A C T

Virtual engine calibration exploiting fully-physical plant models is the most promising solution for the reduction of time and cost of the traditional calibration process based on experimental testing. However, accuracy issues on the estimation of pollutant emissions are still unresolved. In this context, the paper shows how a virtual test rig can be built by combining a fully-physical engine model, featuring predictive combustion and NOx sub-models, with data-driven soot and particle number models. To this aim, a dedicated experimental campaign was carried out on a 1.6 liter EU6 diesel engine. A limited subset of the measured data was used to calibrate the predictive combustion and NOx sub-models. The measured data were also used to develop data-driven models to estimate soot and particulate emissions in terms of Filter Smoke Number (FSN) and Particle Number (PN), respectively. Inputs from engine calibration parameters (e.g., fuel injection timing and pressure) and combustion-related quantities computed by the physical model (e.g., combustion duration), were then merged. In this way, thanks to the combination of the two different datasets, the accuracy of the abovementioned models was improved by 20% for the FSN and 25% for the PN. The coupled physical and data-driven model was then used to optimize the engine calibration (fuel injection, air management) exploiting the Non-dominated Sorting genetic algorithm. The calibration obtained with the virtual methodology was then adopted on the engine test bench. A BSFC improvement of 10 g/kWh and a combustion reduction of 3.0 dB in comparison with the starting calibration was achieved.

1. Introduction

Nowadays, the emissions regulations enforcement combined with the need of meeting the highly demanding targets in terms of CO2 reduction, are pushing the Original Equipment Manufacturers (OEMs) not only towards an unprecedented appeal to powertrain electrification, but also to the introduction of innovative technologies in modern powertrains [1,2]. These complex subsystems (boosting [3,4], valve-train [5,6], aftertreatment [7–9]) have been demonstrated to be capable to improve fuel efficiency and reduce exhaust emissions. However, their control and optimization introduce several degrees of freedoms and additional challenges in the engine calibration, an expensive and time-consuming task, in the context of an increasingly competitive aggressiveness of the automotive sector which is aiming for a shorter time-to-market [10].

In this framework, virtualization can play a fundamental role during the engine development process, minimizing the need of prototypes, and reducing the experimental testing. However, virtualization leverages on the reliability and accuracy of fully-physical plant models, usually built and validated considering a reduced set of experimental data [11,12]. The development of such fully-physical models allows to predict the engine operation even in off-design conditions, thus moving the assessment of design definition and the calibration task much earlier in the engine development process. In addition, considering both the intrinsic low-cost parallelization capability and the constant increment of the computing technology, they guarantee to consistently shorten the lead time to scrutinize several parameters combinations by means of Design of Experiment (DoE) and optimization techniques [13,14]. Indeed, modern compression ignition (CI) engines feature extremely complex control strategies and hardware solutions: fuel injection systems are nowadays capable to provide up to 10 injection events per engine cycle; Exhaust Gas Recirculation (EGR) is typically based on a double path; air management usually relies on multi-stage

---

Acronyms

AI	Artificial Intelligence
ANN	Artificial Neural Network
APC	AVL Particle Counter
BMEP	Brake Mean Effective Pressure
BSFC	Brake Specific Fuel Consumption
BSNOx	Brake Specific NOx
bTDCf	Before Top Dead Center Firing
CAC	Charge Air Cooler
CI	Compression Ignition
CN	Combustion Noise
CO	Carbon Monoxide
CPU	Central Processing Unit
DOC	Diesel Oxidation Catalyst
DoE	Design of Experiment
DPF	Diesel Particulate Filter
ECU	Electronic Control Unit
EGR	Exhaust Gas Recirculation
ET	Energizing Time
FFNN	Feed Forward Neural Network
FFT	Fast Fourier Transform
FRM	Fast Running Model
FSN	Filter Smoke Number
FTP-75	Federal Test Procedure
GA	Genetic Algorithm
HC	Unburned Hydrocarbons
HiL	Hardware-in-the-loop
IMEP	Indicated Mean Effective Pressure
k-NN	k-Nearest Neighbor
KP	Key-point
LM	Levenberg-Marquardt
LP	Low-pressure
MFB	Mass Fraction Burned
MLP	Multi-Layer Perceptron
MSE	Mean Squared Error
NCA	Neighborhood Component Analysis
NSGA	Non-dominated Sorting Genetic Algorithm
OEM	Original Equipment Manufacturers
PCC	Pearson Correlation Coefficient
PN	Particle Number
RDE	Real Driving Emissions
RMSE	Root Mean Square Error
RTF	Real-Time Factor
SCR	Selective Catalytic Reduction
SM	Smokemeter
SOI	Start Of Injection
VGT	Variable Geometry Turbine
WLTC	Worldwide Harmonized Light Vehicles Test Cycle

Symbols

μ	Mean
ρ	Pearson correlation coefficient
σ	Standard deviation
b_j	Neurons biases
n	Number of inputs features
N	Scalar observations
M	Layer neurons
R	Pearson correlation coefficient matrix
w_0	Output layer weights vector
w_{jk}	Neurons coefficients

turbochargers that are often coupled with variable valve actuations. Therefore, the engine calibration process is becoming an extremely complex task, since calibration engineers should define more than dozen control parameters as a result of a highly non-linear optimization problem, in which the dependent variables (i.e., as fuel consumption, emissions and noise) are competing targets. As widely reported in literature, even considering specific DoE methodologies in conjunction with dedicated objective functions [15–17], the standard engine calibration procedure usually involves large experimental campaigns which are extremely expensive and time-consuming. In addition, Real Driving Emissions (RDE) requirements make this task even more complex, since calibration must take into account operating conditions which are usually not available in a conventional engine test bench as altitude, cold and hot environments, thus making standard approaches based on data-driven model developed on local DoE simply inapplicable.

Therefore, in the last decade engine calibration exploiting virtual approaches is becoming of increasing interest, as widely reported in a recent review from Yu et al. [18]. In [19], a nonlinear statistical dynamic modeling, based on measurements, has been developed and applied to the virtual calibration of a gasoline engine, highlighting a trade-off between calibration accuracy and time. However, the authors showed an almost flat trade-off, in which the accuracy worsening is usually very limited thus being almost negligible considering the remarkable savings in calibration and measurement time. A coupling approach between 1D-CFD fully-physical model and a multipurpose commercial optimizer has been exploited by Bozza et al. [20], with the aim to identify the best engine calibration in terms of fuel consumption minimization at part load, acting on the intake valve closure angle, the throttle valve opening, the turbocharger settings, and the spark timing. A virtual methodology for the ECU (Engine Control Unit) calibration has been developed by Grasreiner et al. [21], based on a turbulence and phenomenological combustion models. Exploiting a slightly different approach, several research activities available in literature are focused on data-driven approaches for modelling engine performance and emissions [22,23]. The development of such models usually relies on a considerable amount of data, jeopardizing the potential of the virtual approach in reducing time-consuming and costly experimental activity. To partially solve this issue, fully-physical models can be adopted since their development requires only a reduced set of experimental data thanks to their intrinsic physical background [24,25]. However, as far as soot emission is concerned, physical models are not able to provide accurate predictions even considering the great efforts made in the last few decades in the understanding of the mechanisms and phenomenology of soot formation and oxidation [26]. More specifically, when empirical and semi-empirical models are coupled with fast running engine models, they guarantee only a qualitative agreement with experiments [27]. Differently, detailed soot models based on chemical reaction schemes are able to accurately predict soot emissions, but their computational time request is not suitable considering the available time for the engine calibration task [28]. Therefore, a different approach needs to be defined. This approach should account not only soot emission, but also particle number (PN), exploiting the potential of the Artificial Intelligence (AI). In 2004, He et al. have chosen the Artificial Neural Network (ANN) approach to develop a simulation tool able to estimate several powertrain quantities including NOx and soot emissions [29]. Similarly, Alonso et al. combined the powerful ANN estimation capability with a Genetic Algorithms (GA) optimization to reduce diesel engine emissions maintaining constant (or even improving) the engine fuel consumption [30]. In 2018, Uslu et al. used an ANN model to estimate several quantities such as brake specific fuel consumption (BSFC), exhaust gas temperature, NOx, unburned hydrocarbons (HC), CO and smoke [31]. These are only few examples of how the ANNs have been chosen for their

Table 1
Main features of the engine test case.

Engine type	4-cylinder DI turbocharged diesel EU6
Engine displacement	1598 cm3
Stroke x Bore	80.1 mm x 79.7 mm
Compression ratio	16:1
Turbocharger	Single-stage with VGT
Fuel injection system	Common rail with solenoid injectors
EGR path	Cooled dual loop circuit
Aftertreatment system	DOC + DPF
Rated Power	100 kW @ 4000 rpm
Rated Torque	320 Nm @ 2000 rpm

capacity to achieve fast and effective estimation results without having any knowledge of the Eq.s that govern the specific system.

In this context, this paper shows how, coupling well-known physical 1D engine models featuring predictive combustion and NOx emission sub-models with a data-driven model for the estimation of soot emissions, a powerful virtual test rig can be built and then used for powertrain virtual calibration activities with limited requirements in terms of experimental data. This work moved from an already developed and validated GT-SUITE model featuring a 1.6-liter diesel engine Fast Running Model (FRM) with DIPulse predictive combustion and NOx emissions model [32]. The engine model was coupled with data-driven soot and particle number models, exploiting an ANN approach for its ability to model non-linear and highly complex systems. With this approach, the Authors were able to gather a reliable and quantitative assessment of engine efficiency and emissions with respect to engine calibration parameters. Then, the engine model was used to optimize the engine calibration in a fully automated way, exploiting NSGA-III (Non-dominated Sorting Genetic Algorithm) and strong parallelization capabilities, considering different design constraints, as the combustion noise. Output of the multi-objective optimization was the Pareto front BSFC- combustion noise, with constraints in terms of soot, particle number and NOx emissions. This result was then used to select the most appropriate calibration set and, eventually, validated at the test bench, clearly highlighting the potential of the proposed approach. Thanks to the exploitation of the predictive capabilities of the fully physical engine coupled with a data-driven approach for soot emissions and particle number, this paper demonstrates the capability to virtually optimize engine calibration moving this task much earlier in the vehicle development process, at a fraction of time and cost in comparison with conventional experimental procedures.

2. Test case

2.1. Engine test case

The selected engine is a 4-cylinder 1.6 liter passenger car diesel engine already presented in [32,33]. To quickly recall its main features, the engine is equipped with a common rail injection system with latest generation 8-holes solenoid injectors capable to work up to 2000 bar injection pressure. The charging system features a Variable Geometry Turbine (VGT) turbocharger with an air-to-air Charge Air Cooler (CAC) and a variable swirl flap. The CAC was replaced with an electrically controlled water-to-air heat exchanger in the engine test bench to independently control the CAC outlet temperature. As far as EGR is concerned, the engine is equipped with a dual loop (high- and low-pressure) cooled EGR, with the high-pressure mainly used at low load and during the warm-up phases, while the low-pressure one is used in normal operating conditions. Since this work focuses on warm steady-state conditions, the high-pressure circuit was not considered. For what concerns the aftertreatment, the engine is equipped with a close-coupled Diesel Oxidation Catalyst (DOC) and a Diesel Particulate Filter (DPF) device, plus a Selective Catalytic Reduction (SCR) underfloor in vehicle configuration. In the dyno setup the underfloor SCR
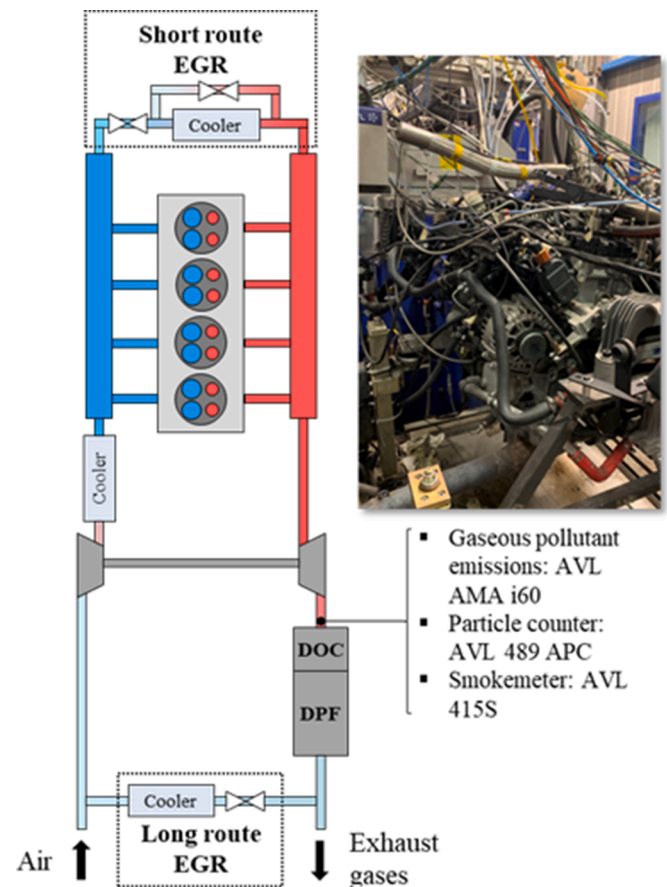

Fig. 1. Engine and emissions sampling layout.

system was replaced with a backpressure valve. Main features of the engine are also reported in Table 1.

2.2. Experimental setup

The engine was tested in the AVL highly dynamic test bench of Energy Department of Politecnico di Torino. Those facilities are deeply described in [34] and schematically depicted in Fig. 1.

The cabin is equipped with a conditioning system to control cabin temperature and intake air humidity and temperature. The engine under test is connected to a highly dynamic AVL DynoExact rated 500 Nm and 200 kW. The fuel consumption is measured via an AVL KMA4000 fuel flow meter. The facilities also include a two-line AVL AMAi60 emission analyzer to measure NO, NOx, HC, CO, CO_2 and O_2 concentrations independently. Eventually, a third line only for CO_2 is available, used to trace EGR. For this specific application, an AVL 415S G002 SmokeMeter (SM) and an AVL 489 Particle Counter (APC) were setup to sample engine out. The first is used to measure Filter Smoke Number (FSN) and the latter to measure the particle number concentration. This instrument has a built-in conditioning unit which uses a twin stage dilutor, and the Dilution Ratio (DR) was set to correctly exploit the measuring range of the device according to the PN emission level. The measuring apparatus is also equipped with an AVL X-ion system to measure in cylinder pressure traces by means of a high frequency AVL piezoelectric pressure transducer (GU 13P AVL) and the solenoid injector current command by means of a high frequency current clamp. Finally, the whole test bench equipment is managed by AVL Puma 2 and AVL Cameo V5 automation software suite.
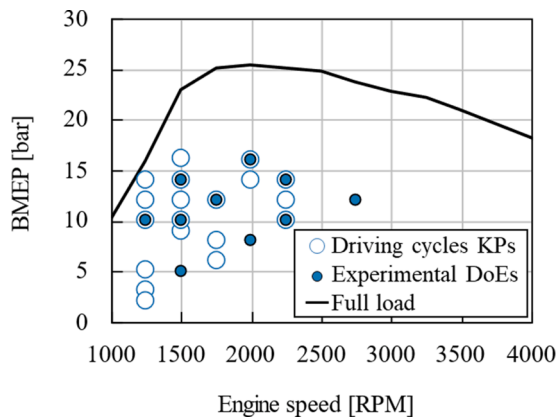
Fig. 2. Experimental test matrix and KPs selection.

2.3. Test matrix

To generate a comprehensive dataset for developing the data-driven models, a dedicated experimental campaign was carried out: in total 10 DoEs (200 points each) spread in the engine map were measured. The selection of the Key Points (KPs) originates from a previous work considering different driving cycles (WLTC, RTS-95, FTP-75 and US06) to identify the most significant operating points within the engine map [32]. Output of that analysis is reported in Fig. 2, in which the selected DoEs are plotted over the abovementioned operating points. As shown, most of the DoEs were chosen within the selected operating points, while few are chosen outside to uniformly cover the whole engine map given the scope of producing a virtual test rig able to represent the engine.

Within each DoE, the main engine calibration independent variables were varied according to the data reported in Table A. 1 in the Appendix. Latin Hypercube DoE sampling technique was chosen as it is more appropriate for ANN training, as suggested in [35].

3. Model overview

3.1. Engine performance model

Since the aim of the present study was to develop a virtual calibration methodology to be applied to a wide number of operating points and calibration sets, the FRM engine developed in [32] has been adopted. The FRM is a 1D-CFD engine model, representative of the 1.6-liter diesel engine object of the work, with a Real Time Factor (RTF) equal to 3. As shown in [36], this level of discretization is Real-Time capable on a HiL (Hardware-in-the-loop) machine [37,38], so no further simplification would be practically useful for engine virtual calibration purposes. More detailed information about this engine model can be found in previous articles [32,33] . However, the most significant features of such engine model are reported in brief.

First, a map of injector profiles corresponding to several Energizing Time (ET) and rail pressure values covering the whole injector working range, was created, as presented in [11]. During engine operation, the injected mass (or ET) and rail pressure are provided as inputs to lookup the corresponding injection rate profile. It is worth to point out two main assumptions which may affect the outcome of the virtual calibration. On the one hand, each injection event is defined as a single pulse for a specified combination of injection pressure and ET, thus not accounting for possible interaction between consecutive injection events (i.e., pulse-to-pulse interaction). On the other hand, dynamic phenomena in the injection system are not considered. Then, the DIPulse predictive combustion model, developed by Gamma Technologies, was used to predict the combustion rate and, by means of Zeldovich Extended Mechanism, also NOx emissions [27,39]. Additionally, a previously calibrated flow model [39] to compute turbulence quantities was

implemented. Soot emissions in terms of FSN and particulate number were computed by the ANN that will be described in detail in the next paragraph. The adoption of a dedicated data-driven approach to model soot emissions is due to the fact that soot formation and oxidation are extremely complex phenomena, and the ANN is able to accurately model non-linear problems, requiring a computational time much lower than detailed 3D-CFD approach. Moreover, to compute the combustion noise, a previously developed user subroutine [13,14] was adopted. This subroutine evaluates the power spectrum of the cylinder pressure signal through a Fast Fourier Transform (FFT) considering attenuation introduced from both the engine structure and the human ear [40,41]. The engine model was operated in steady state conditions and controlled by means of fuel injection, EGR valves (low- and high-pressure) and VGT controllers targeting the desired load, EGR rates, and the boost pressure. The engine model was then calibrated over a subset of 29 operating points and validated with respect to the experimental data obtained by the test campaign. The engine operating points selected for the calibration and the results of the model validation in terms of calibration error have been presented in a previous work [42].

Taking advantage of the predictive combustion model DIPulse and the in-cylinder turbulence model, it was possible to estimate several combustion and turbulence-related quantities which are not normally measured and computed by the Electronic Control Unit (ECU) during engine operation. As an example, in this activity the liquid spray penetration, several indices of the heat release shape, swirl number and burned gas temperature at various combustion instants have been considered. Those quantities are strongly related to the soot formation and oxidation phenomena, and are fed, together with all the other measured quantities to the features selection algorithm to define the input list for the data-driven soot mode. In traditional approaches for virtual calibration those inputs are not normally available since a comprehensive physical combustion and turbulence model is not used. In the Appendix, the complete list of the ECU-related and combustion-related features are reported in Table A.2.

3.2. Data-driven FSN and PN models

In this section the methodology to develop the data-driven models for FSN and PN estimation, is reported. First, among several engine variables, a reduced set of independent variables (also known as features) is selected. Then, the ANN model is trained and validated with respect to experimental data.

3.2.1. Independent variables selection

In a regression problem, a fundamental step is the so-called feature selection: starting from a large dataset, the selection procedure goal is to identify an input feature-set that minimizes the model complexity, maximizing its performance. A feature set can be defined as "well chosen" if composed by relevant and non-redundant inputs. More specifically, a feature is considered as relevant if it is correlated (linearly or not-linearly) with a target variable, while it is considered redundant if it is highly correlated with one or more features

In this project, the data-driven model inputs were selected within a pool of 62 variables, including actuators commands and FRM outputs. The variables pool was identified by selecting from the engine operation standpoint quantities related to EGR and lambda control (e.g., valves position, boost, swirl flap position) and combustion control (e.g. injection pressure, injection pulses phasing and injection durations). Together with those, in cylinder quantities calculated ex-post from in cylinder pressure trace analysis were selected, for example combustion phasing (start of combustion, various angles at a given mass fraction burned) and various thermodynamic snapshot taken at different crank angles of the engine cycle. The general idea behind the variable selection is to feed the features selection algorithm with a set of variables describing comprehensively the combustion process leaving the algorithm to select the most relevant for the soot formation phenomenon.
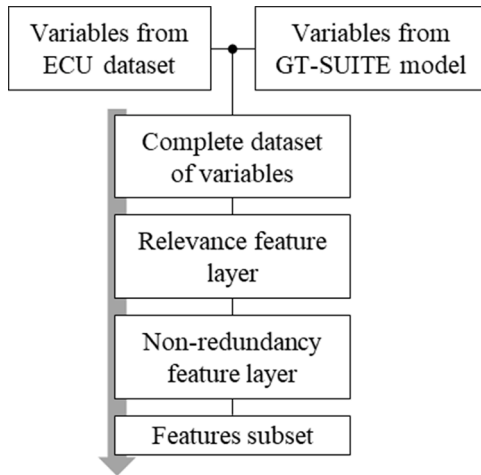
Fig. 3. Features Selection Schematic.

Table 2
PCC coefficients interpretation.

Values	Correlation
$\pm 0.9 \rightarrow \pm 1$	Almost linear (positive/negative)
$\pm 0.7 \rightarrow \pm 0.9$	High (positive/negative)
$\pm 0.5 \rightarrow \pm 0.7$	Moderate (positive/negative)
$\pm 0.3 \rightarrow \pm 0.5$	Low (positive/negative)
$\pm 0 \rightarrow \pm 0.3$	Negligible (positive/negative)

Going back to the feature selection algorithm, as schematically depicted in Fig. 3, starting from the combined dataset, the following layers were implemented:

- Relevance Feature Layer: the Neighborhood Component Analysis (NCA) with L2 Regularization have been implemented to identify the capability of inputs to predict the target.
- Non-Redundancy Feature Layer: the Pearson Correlation Coefficients have been calculated to identify features redundancies.

The NCA is the learning algorithm used to highlight the optimal informative input subset. The NCA is a non-parametric method for selecting features based on the k-Nearest Neighbor (k-NN) algorithm. The output of the implemented procedure is the ranking of the features, that minimize the k-NN regression problem.

As far as the identification of features redundancies is concerned, the Pearson Correlation Coefficient has been used. In general, the correlation coefficient between two random variables is a measure of their linear dependence. If each variable has N scalar observations, then the Pearson Correlation Coefficient (PCC) is defined as reported in Eq. 1:

$$\rho(A,B) = \frac{1}{N-1} \sum_{i=1}^{N} \left(\frac{A_i - \mu_A}{\sigma_A} \right) \left(\frac{B_i - \mu_B}{\sigma_B} \right) \qquad \text{(Eq. 1)}$$

where μ_A and σ_A are the mean and standard deviation of A, respectively, and μ_B and σ_B are the mean and standard deviation of B. The PCC matrix of two random variables is the matrix of correlation coefficients for each pairwise variable combination is defined in Eq. 2:

$$R = \begin{pmatrix} \rho(A,A) & \rho(A,B) \\ \rho(B,A) & \rho(B,B) \end{pmatrix} \qquad \text{(Eq. 2)}$$

Since A and B are always directly correlated to themselves, the diagonal entries are equal to 1, therefore the PCC matrix is shown in Eq. 3:

$$R = \begin{pmatrix} 1 & \rho(A,B) \\ \rho(B,A) & 1 \end{pmatrix} \qquad \text{(Eq. 3)}$$

Table 3
Variables selected for the data-driven emission models development.

|	Variable #	Variable description
ECU variables	1	Energizing Time of Main Injection
	2	Start of Main Injection
	3	Energizing Time of Pilot 1 Injection
	4	Energizing Time of Pilot 2 Injection
	5	Rail Pressure
	6	Swirl Flap Position
	7	VGT Position
	8	Low Pressure EGR Valve Position
GT-SUITE variables	9	In-Cylinder Trapped O2 Mass
	10	MFB90 (Crank Angle at 90% Mass Fraction Burned)
	11	Burned Gas Temperature at MFB90
	12	Swirl Ratio at MFB90
	13	Exhaust Manifold Temperature
	14	EGR Rate
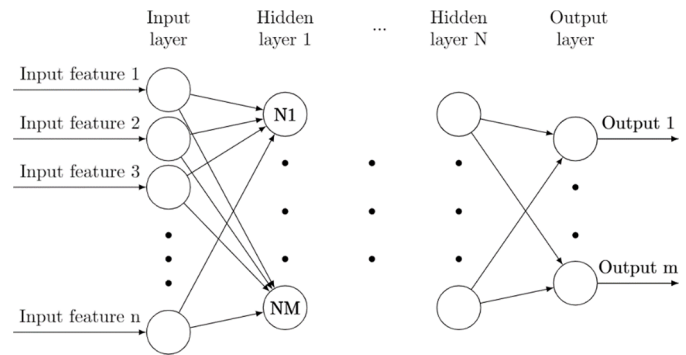
Fig. 4. Feed-Forward Neural Network structure.

The interpretation of the PCC coefficients is reported in Table 2, as defined in [43]:

The PCC layer computes the correlation coefficients between each feature and selects the variables with a correlation value greater than 0.9. The winner redundant variable is the one with the best score in the informative ranking of the previous layer.

The optimal subset output of the previously described two-stage filter is summarized in Table 3 where variables are divided in "ECU variables", inputs normally available within engine ECU, and "GT-SUITE variables", computed by the engine model. It should be highlighted that these latter ones are, in fact, variables that the physical engine model can compute but, in order to get rid of the combustion model inaccuracies, for the training of the neural networks, the corresponding experimental values computed by the post processing of the in-cylinder pressure traces have been used. Moreover, to assess the benefit from this combined approach, the same procedure was followed considering only ECU variables.

3.3. Neural network architecture definition

Among the state-of-the-art of ANNs possibilities, a Multi-Layer Perceptron (MLP) or Feed Forward Neural Network (FFNN) was selected [44,45]. The choice was driven by the following requirements:

- Complex and non-linear mapping from inputs to output;
- Steady-state estimation.

The FFNN output can be interpreted as the concatenation of N vector-valued functions called layers. A standard FFNN structure is depicted in Fig. 4.

It is shown that layers are fully-connected and are divided into one input layer, multiple hidden layers, and one output layer. Each layer is a
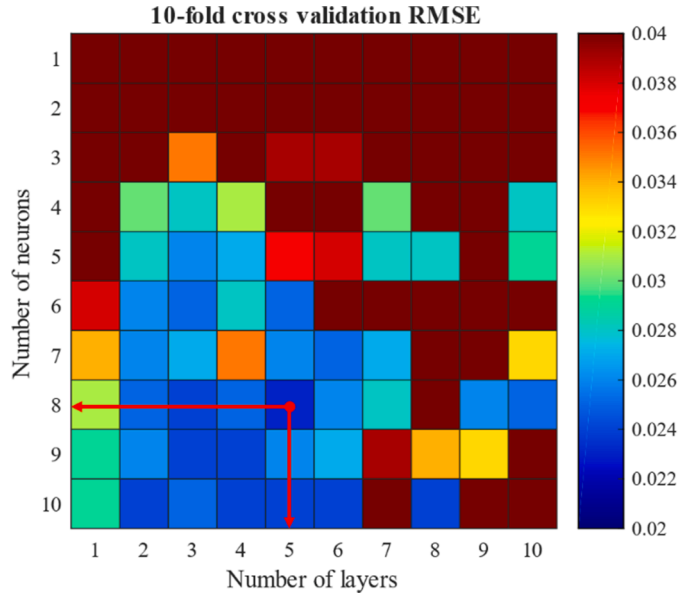
Fig. 5. 10-Fold Cross Validation Grid Search.

Fig. 6. PN and FSN regression plot of the ANN comparing ECU-only (top) and ECU+GT (bottom) approaches.

collection of M scalar-valued functions, where a single node is a computational unit known as a neuron. Neurons introduce nonlinear transformation, exploiting particular activation functions $h(x)$. The outputs of the first hidden layer are computed as shown in Eq. 4, where n is the number of inputs features and M is the total layer neurons.

$$z^{(1)}(w, x) = z_j^{(1)}(w, x) = h\left(\sum_{k=1}^{n} w_{jk}x_k + b_j\right), j = 1, 2, ..., M \qquad \text{(Eq. 4)}$$

Thus, in the case of a scalar target, the output for a regression problem is given by Eq. 5, where N is the net total number of layers and w_o is the output layer weights vector.

$$\widehat{y}(w, x) = z^{(N)}\left(z^{(N-1)}\left(\ldots z^{(1)}(w, x)\right)\right)^T w_o \qquad \text{(Eq. 5)}$$

Total neurons M, layers N and activation function type are designer choices called hyper-parameters. The net identifies an input/output relationship using a supervised learning method named back-propagation. The neurons coefficients w_{jk} and biases b_j are the optimization variable adjusted to minimize the Mean Squared Error (MSE) between actual and estimated values.

3.3.1. Neural network model configuration

During neural network configuration definition, one of the most common challenges is the so-called bias-variance trade-off (i.e. the problem of finding the optimal model for estimation as well as for generalization [46]). To avoid this issue, a common method is splitting the whole dataset into a training set and a test set, 80% and 20% respectively.

Firstly, the Hyperbolic Tangent (Tanh) was considered as an activation function for its ability to introduce strong nonlinearities avoiding saturation [47] . Secondly, a 10-Fold Cross-Validation Grid Search on the number of layers and their total neurons was performed to select the optimal network architecture [48]. A representative grid is reported in Fig. 5. The optimal solution has been chosen as the one with minimum Root Mean Square Error (RMSE) across the 10 folders. The best architecture was composed of 5 layers with 8 neurons each.

Levenberg-Marquardt (LM) optimization with Bayesian Regularization was used as learning algorithm. Input data was scaled between ± 1 preserving the shape of the original distributions. To enhance regression performance and reduce optimization convergence time, the Nguyen-Widrow layer initialization function was used. Finally, the training data set was exploited to find the best network model of the above-
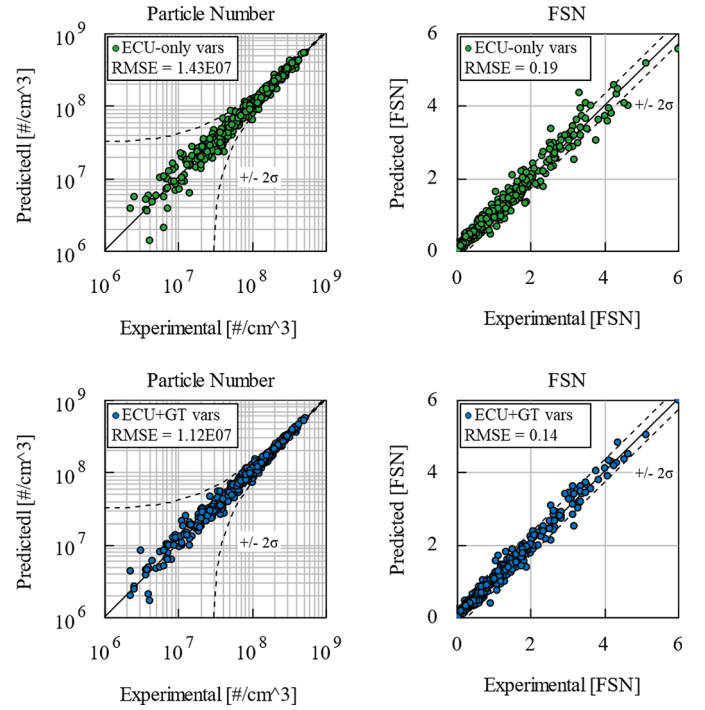
mentioned optimal architecture. Due to the slight randomness introduced by the initialization algorithm, the network was trained and tested 10 times, each time using a different value for the pseudo-random number generator. The model with minimum RMSE was chosen.

3.3.2. Performance evaluation

As previously introduced, to benchmark the classical approach in which the emission models are fed by engine actuators setpoint only (from here on referred as "ECU-only" approach since the used inputs are normally available within engine ECU) and the proposed approach in which the information from the physical engine model are added (from here on referred as "ECU+GT"), the models have been retrained excluding the engine model inputs while keeping the same total number of inputs.

The quality of the developed NN have been assessed over the 20% remaining testing dataset. The considered observations have been kept aside before training and validation so that model performances have been evaluated in terms of generalization capability. Regression results have been reported in Fig. 6 comparing ECU-only and ECU+GT approaches. As shown, the wide majority of the points are within the 95% confidence interval of the experimental measurement computed by analyzing DoEs repetition points. Moreover, moving from ECU-only to ECU+GT inputs, the RMSE value improves by 21% for Particle Number and 26% for FSN confirming the potentialities of this approach.

Moreover, experimental activities have also provided a set of actuators position sweep variations to further assess the capability of the models to follow a specific physical trend. Comparison of experimental and simulated FSN and PN values as a function of the actuator setpoint, are reported in Fig. 7 and Fig. 8 respectively. The experimental value is always well reproduced, and the trends are well captured for both models even though the PN model seems more accurate and robust. In fact, it is worth to note that FSN shows deviation up to $0.5 - 0.75$ FSN in specific conditions at low injection and low boost pressures.

3.3.3. Sensitivity on observations and on independent variables

To better analyze the performance of the ANN, a sensitivity analysis has been performed varying the number of training data and feature
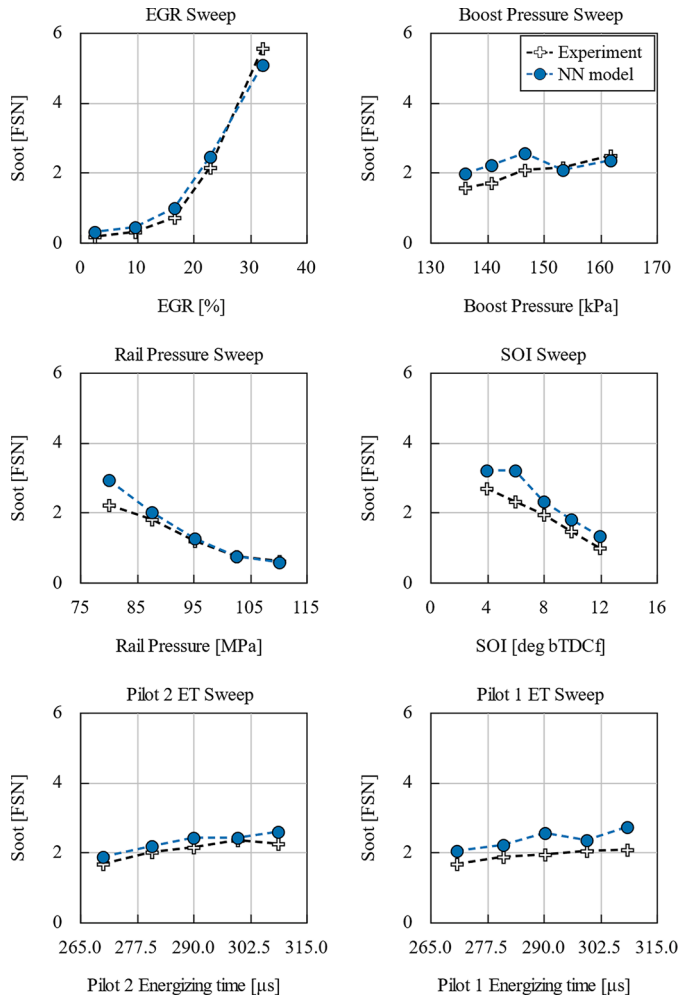
Fig. 7. FSN from experiments and the ANN model prediction for different sweeps of engine parameters.

Fig. 8. Particle Number from experiments and the ANN model prediction for different sweeps of engine parameters.

inputs. In particular, the design dataset has been reduced up to 500 samples and the NN inputs have been reduced deleting the features with the lowest ranking values (up to 7).

The outcome of this analysis is summarized in Fig. 9. In this Fig. the probability density function of the difference between the predicted and experimental soot (i.e., the prediction error) is reported for three analyzed combinations of number of samples and variables. It is noticeable that the increase of both training points and number of independent variables significantly reduce the error, narrowing the distribution close to the zero-error line. When the number of training points is limited (500), the distribution becomes wider highlighting limited benefit when the number of variables grows from 7 to 14. Moreover, a reduction of samples or independent variables moves the distribution mode away from the zero-error line, thus resulting in a higher average error on the whole dataset.

Extending the analysis to the whole matrix, the results in terms of RMSE for each combination of number of samples and variables are shown in Table 4. It is worth to point out that focusing on the extended dataset (i.e., 1616 training points) an increase of the number of variables to 11 or 14 is beneficial to reduce the RMS error, thus justifying the selection of 14 independent variables.

3.4. Integration and validation

After validating the standalone FSN and PN models, they have been compiled into .dll and integrated in the GT-SUITE model. If in the
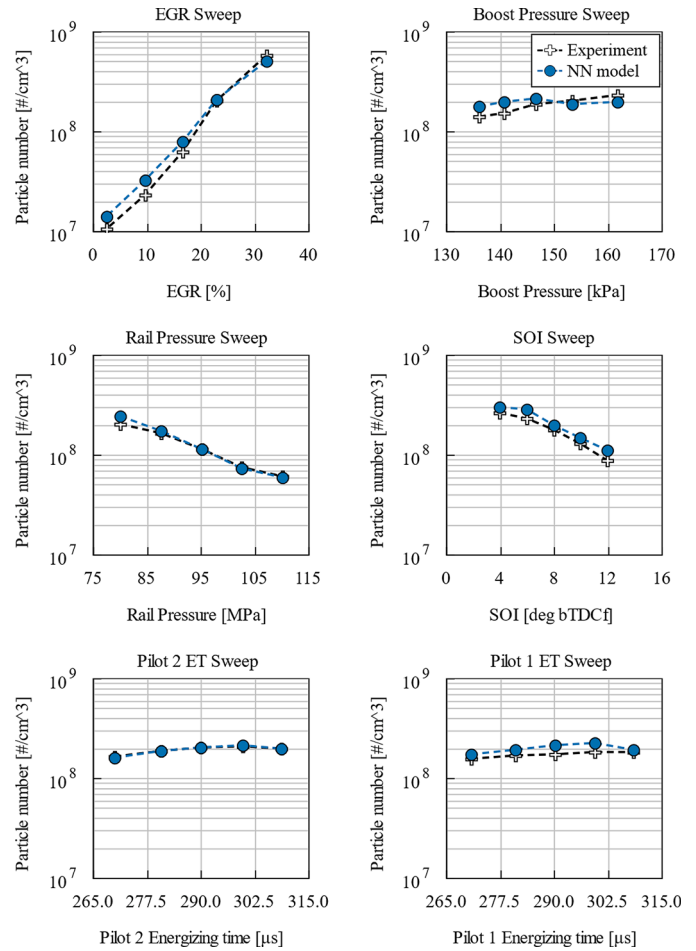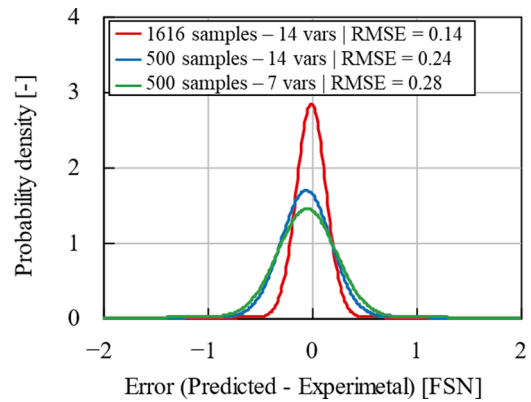

Fig. 9. Probability density function of the FSN model error considering different combinations of number of samples and variables.

Table 4
FSN model RMSE considering different combinations of number of samples and variables.

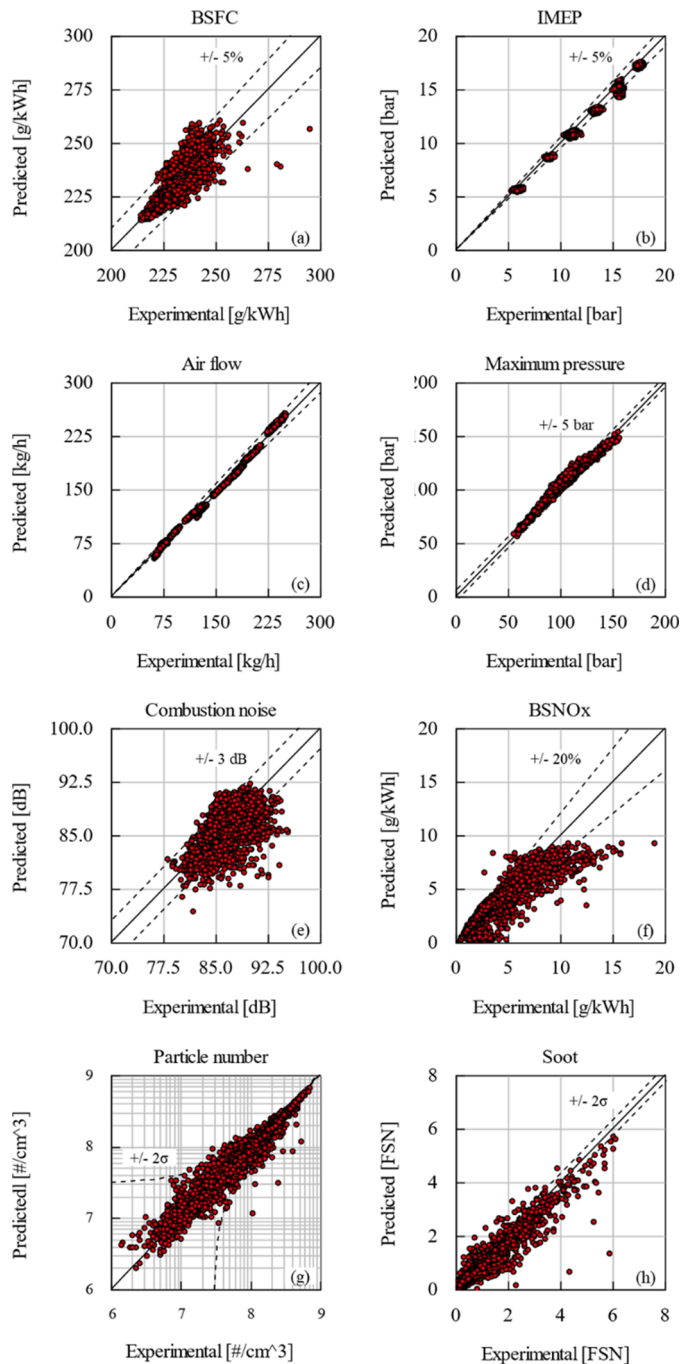| Samples \ Variables	7	11	14
500	0.28	0.25	0.24
1000	0.23	0.18	0.18
1616	0.18	0.17	0.14

Fig. 10. GT-SUITE and ANN integrated model correlation assessment: BSFC (a), IMEP (b), air flow (c), maximum in-cylinder pressure (d), combustion noise (e), BSNOx (f), particle number (g), filter smoke number (h).

Table 5
Optimization of the engine calibration - Ranges of the independent variables.

Variable	Unit	Lower Limit	Upper Limit
Low-Pressure EGR Rate	%	0	30.5
Boost Pressure	bar	1.35	1.69
Rail Pressure	bar	740	1100
Fuel Quantity Pilot Injection 1	mg	1.3	3
Fuel Quantity Pilot Injection 1	mg	1.3	3
Start of Injection Main	°aTDCF	-12	0.1
Δ Start of Injection Pilot 1	°	10	25
Δ Start of Injection Pilot 2	°	10	25

error band, and maximum in-cylinder pressure is well-predicted with an error that lies within 5 bar tolerance. The prediction for combustion noise is less accurate and will be the matter of future studies, however for more the 70% of the measured points the error is within +/- 3dB. Moving to pollutant emissions, the prediction quality of the Extended Zeldovich NOx model is in line with the results presented in previous works [11,27,36], within 20% error band for more than 70% of the measured points. For what concerns the results of the integrated neural networks model for FSN and PN, due to inputs inaccuracies, now computed by the physical engine model, the results are slightly worse with respect to what presented in the ANN validation section for the test dataset (Fig. 6). Here, the RMSE increases up to 3E7 for PN and up to 0.36 for FSN. As future work, the ANN models will be trained using the output of the engine model to evaluate if the data-driven model can guarantee same or similar results quality compensating the inaccuracies of the physical engine model.

4. Calibration optimization

In this section, the methodology for the optimization of the engine calibration and the subsequent experimental validation, on a single operating point at 2000 rpm and 8 bar of BMEP, is reported.

The optimization of an engine calibration is the results of trade-offs among several engine responses. Commonly, the optimal calibration is chosen among various solutions within the design constraints (e.g., limits in PN, FSN, combustion noise). In this work, a multi-objective optimization solved by the metaheuristic algorithm NSGA-III (Non-dominated Sorting Genetic Algorithm) was adopted. Moreover, the optimization was set to define a Pareto front of equally optimal solutions. Among these, the best-fit calibration could be selected. This optimization setting proved to be efficient for virtual engine calibration analysis as reported by Millo et al. [32] and was therefore used for this analysis.

For this work, the independent variables considered are 8: namely SOI and injected mass of the main injection and two pilot injections, the EGR rate of the low-pressure circuit (the high-pressure EGR has been imposed equal to zero), the boost pressure and the rail pressure. The range of the optimization parameters for the selected operating point is reported in Table 5. The fuel quantity of the main injection is the output of the fuel injection controller to achieve the target load. Instead of directly optimize the VGT and EGR valve position, the boost pressure and the low-pressure EGR (LP-EGR) rate have been adopted as independent variable for the optimizer. Indeed, the engine model includes a EGR and a VGT controller, which act on LP-EGR valve and VGT position respectively, to achieve the target set by the optimizer.

Among the results of the optimization, the calibration sets that do not satisfy the constraints of torque (with a tolerance of ± 5 Nm), and the BSNOx, FSN and PN maximum prescribed limits for the given operating point, are discarded from the results. FSN and PN are estimated by the data-driven model.

As settings for the GA optimization, a population size of 100 members and a number of generations equal to 40 are chosen. These settings provide that, at the end of the optimization (i.e., after 4000 iterations), even considering iterations that have to be discarded given engine

standalone NN validation the combustion-related inputs were generated from the experimental measurements (i.e., combustion characteristic angles and temperatures were computed by in-cylinder pressure analysis), in this configuration all the requested inputs are computed by the GT-SUITE engine model.

In Fig. 10, the correlation plots for BSFC, Indicated Mean Effective Pressure (IMEP), air flow, maximum in-cylinder pressure, combustion noise, brake specific NOx (BSNOx), PN and FSN are reported over the full experimental dataset, which contains a total of 2232 operating points. Overall, the agreement between experimental data and model results is satisfactory. Looking at the engine performance-related parameters (i.e., BSFC, Air Flow and IMEP) most of the points is within 5%

Table 6
Optimization Algorithm Settings.

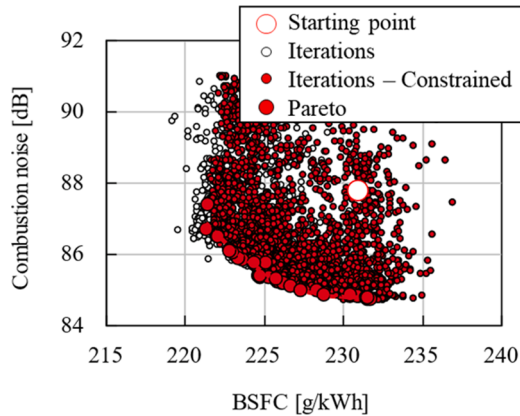|	
Number of independent variables	8
Population size	100
Number of generations	40
Crossover rate (distribution index)	1 (15)
Mutation rate (distribution index)	0.1 (20)

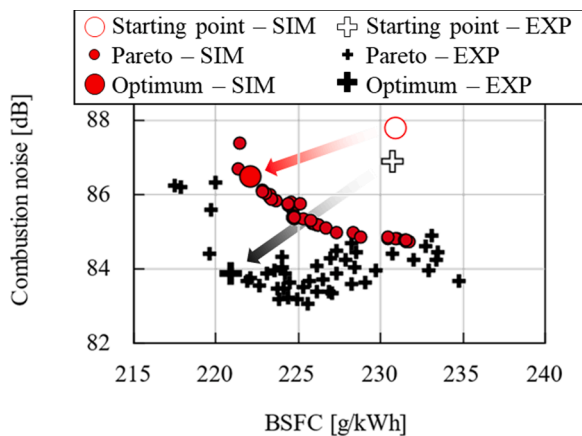**Fig. 11.** Numerical optimization results: BSFC andcombustion noise.

Fig. 12. Experimental validation of the optimization results: BSFC-combustion noise tradeoff.

response outside the design constraints, a sufficient number of potential calibration sets is available. The optimizer took around 5 hours to complete the 4000 iterations using 4 cores on a standard desktop PC (CPU: i7-9700 CPU @ 3.00GHz). The obtained results have been analyzed evaluating the optimal calibration sets on a Pareto front based on BSFC and combustion noise for the operating point under study. The GA settings are reported in Table 6.

4.1. Results

The output of the optimizer is depicted in Fig. 11, where the optimization starting point, intermediate iterations and the resulting Pareto front are reported. As shown, the majority of the iterations lies in a region with lower BSFC and lower CN with respect to the starting point. The optimizer is able to define a Pareto front ranging from 221 to 232 g/kWh of BSFC and 85 to 88 dB of combustion noise.

Since the Pareto front is a continuum with several solutions that can be considered equally optimal, to select the most suitable calibration, a dedicated Eq. to weigh both fuel consumption and combustion noise was

introduced. The weight W_i, reported in Eq. 5, was computed over the selected pareto points i, named 'Pareto' in Fig. 11.

$$W_i = k_{BSFC} \cdot \left(\frac{BSFC_i}{BSFC_{base}} \right) + k_{CN} \cdot 10^{\left(\frac{CN_i - CN_{base}}{20} \right)} \qquad \text{(Eq. 5)}$$

Where, k_{BSFC} and k_{CN} are two calibration constants with the aim to properly weight the two terms of the Eq., the fuel consumption and the combustion noise. In this activity, $k_{BSFC} = 10$ and $k_{CN} = 1$ have been selected.

The experimental validation of the virtual calibration procedure is reported in Fig. 12 and Fig. 13. In Fig. 12 the optimal BSFC-combustion noise tradeoffs selected by the model are compared with the corresponding experiments. It is worth to point out that the experimental cloud is close to the simulated pareto: the BSFC range is the same, while, as expected looking at the correlation plot in Fig. 10, the correspondence of the combustion noise is less accurate, and it also shows an offset of around 1.5-2 dB. Comparing the Starting Point-to-Optimum trajectory demonstrates how the direction taken by the optimizer is confirmed by experimental tests even though, due to combustion noise model inaccuracies, the selected optimal calibration is associated to a 2db lower noise with respect to model prediction at the same BSFC.

Fig. 13 shows the same operating conditions reported in Fig. 12 BSNOx. The BSNOx-FSN plot highlights how the optimization correctly selects calibrations closer to the given constraints. The BSNOx correlation can be considered very good as can be noted by comparing the abscissa of the optimal calibration which is exactly on the prescribed limit. Few experimental points are outside of the NOx limit threshold but inside the 20% model error band reported in Fig. 10. On the other hand, the experimental measurements highlighted a quite clear offset in FSN with respect to the simulated value. As seen in Fig. 7, the FSN predicted by the ANN model shows a deviation that is up to 0.5-0.75 FSN when the engine is operated at low injection and boost pressure. The cause of this offset will be the subject of future studies. This offset is not seen in the particle number-BSNOx tradeoff in which the two clouds and the optimal calibration are almost overlapping, suggesting that the FSN offset issue may also come from a model's robustness problem as shown in the sweep validation plot. Same conclusion can be drawn looking at BSFC-BSNOx tradeoff where the starting point and optimal calibration are perfectly overlapping. Finally, the combustion noise-BSNOx tradeoff plot shows that the noise is overestimated by the virtual test plant as described in Fig. 12.

As a result, the experimental validation showed a BSFC improvement of 10 g/kWh as predicted by the model. At the same time, the combustion noise improved by 3 dB, slightly underestimated by the virtual approach. While the optimizer moved the calibration towards the maximum allowed BSNOx, the FSN increased from 1.5 to 1.7 with no penalties on PN. These results, which are technically sound from a qualitative and quantitative aspect, demonstrate that the developed fully-physical engine model coupled with ANNs for the prediction of FSN and PN can be effectively used for virtual calibration purpose. The advantage of this approach lies in the improvement in terms of time and cost with respect to common calibration techniques. Indeed, the engine testing could be limited to reduced phases before and after the calibration process. Before the calibration process the main task would reduce to the gathering of specific data for the development of the engine model and the training of the ANNs for FSN and PN prediction, while after the virtual calibration process, the experimental tests would be used to validate the best-fit calibration and only perform additional sensitivity analysis.

5. Conclusions

In this work, a methodology for the virtual calibration of a series production diesel engine was proposed to speed-up the workflow commonly followed during engine development activities.
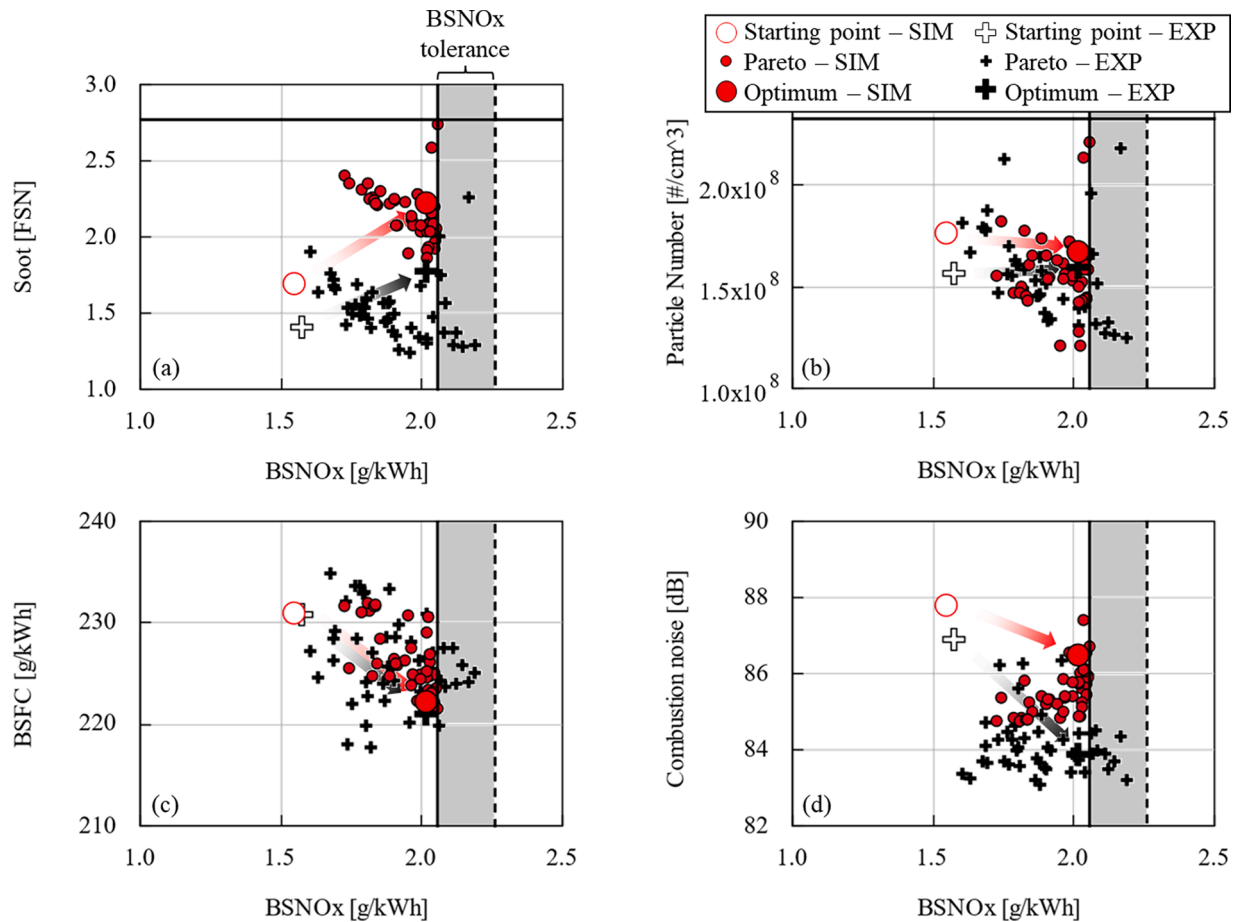
Fig. 13. Experimental validation of the optimization results: FSN (a), PN (b), BSFC (c), combustion noise (d) as a function of BSNOx (NOx tradeoff).

First, a fully-physical model of a 1.6-liter diesel engine featuring predictive combustion and NOx sub-models, was coupled with a data-driven model for soot and PN estimation. Moreover, a user subroutine for the computation of the engine noise was integrated in the model. The development of the soot and PN model leveraged the accessibility of engine model variables, not commonly measurable during experimental testing, linked to the soot formation and oxidation phenomena. This led to the selection of 62 variables, half of which coming from the engine model and half from the Engine Control Unit. A subset of 6 variables coming from the engine model and 8 variables coming from the ECU were finally chosen by means of the Neighborhood Component and Pearson Correlation analyses. Then, a Feed-Forward Neural Network composed by 5 layers with 8 neurons each, was trained and validated over the dataset showing satisfactory results.

Then, the engine model was used as virtual test rig for the optimization of the engine calibration. 8 independent variables were chosen such as EGR rate, boost pressure and main variables related to the fuel injection (injection pulses timing and duration and rail pressure). Taking into account emissions constraints, a genetic algorithm-driven multi-objective optimization was performed minimizing Brake Specific Fuel Consumption (BSFC) and combustion noise. Afterwards, the resulting Pareto Front was experimentally validated showing that NOx and PN limits were accurately predicted by the combined physical and data driven approach, while a slight overestimation of FSN was observed. In comparison with the starting calibration, a BSFC improvement of about 10 g/kWh and a combustion reduction of 1.5 dB was obtained as a result of the optimization process. When the virtually optimized calibration was adopted in a dedicated experimental test, a BSFC improvement of 10 g/kWh and a combustion reduction of 3 dB was achieved, while maintaining BSNOx value below the maximum allowed constraint.

In conclusion, these results demonstrated the reliability of the proposed methodology of virtual calibration for the quantitative assessment of engine fuel consumption, combustion noise and pollutant emissions such as NOx, soot and PN. This methodology addresses the problem of engine calibration exploring thousands of possible combinations at a fraction of time and cost with respect to traditional approaches, providing results that could directly be used by calibration engineers as a complementary tool for the selection of the most appropriate calibration set.

Finally, further investigation will be necessary to extend the data-driven model to other pollutant emissions, such as unburned hydrocarbons (HCs) and carbon monoxide (CO).

Declaration of Competing Interests

The authors declare that they have no known competing financial interests or personal relationships that could have appeared to influence

Table A.1
Experimental engine DOE tests - Ranges of the selected variables.

Variable name	Unit	Min	Max
Rail Pressure	bar	400	1350
SOI Main	CAaTDCf	-12	0
Fresh Air Setpoint (LP-EGR Ctrl)	mg/cyc/cyl	300	800
VGT position	%	50	95
P1 Quantity	mm³	1.3	3
P1 Dwell Time	µs	600	1600
P2 Quantity	mm³	1.3	3
P2 Dwell Time	µs	600	1200
Swirl Flap Position	%	0	60

Table A.2

Features of interest used for the independent variable selection. The features are grouped in ECU variables, Test Bench variables and GT-SUITE variables.

	Variable #	Variable description
ECU variables	1	Dwell Time of Pilot 1 Injection
	2	Dwell Time of Pilot 2 Injection
	3	Energizing Time of Main Injection
	4	Energizing Time of Pilot 1 Injection
	5	Energizing Time of Pilot 2 Injection
	6	Start of Main Injection
	7	Fuel Volume of Main Injection
	8	Fuel Volume of Pilot 1 Injection
	9	Fuel Volume of Pilot 2 Injection
	10	Ambient Pressure
	11	Intake Manifold Pressure
	12	Swirl Flap Position
	13	Accelerator Pedal Position
	14	VGT Position
	15	Computed Exhaust Volume Flow Rate
	16	Engine Coolant Temperature
	17	DPF Pressure Drop
	18	Upstream DOC Exhaust Gas Temperature
	19	Upstream DPF Exhaust Gas Temperature
	20	Downstream DPF Exhaust Gas Temperature
	21	Intake Manifold Temperature
	22	Engine Oil Pressure
	23	Engine Oil Temperature
	24	Engine Speed
	25	Friction Torque
	26	Fuel Rail Pressure
	27	Injected Fuel Volume
	28	Low Pressure EGR Valve Position
	29	In-Cylinder Trapped Air Mass
	30	Compressor Pressure Ratio
	31	Throttle Valve Position
Test Bench Variables	32	Air Relative Humidity
	33	Exhaust Gas Temperature
	34	EGR LP Mixing Point Temperature
	35	Engine Coolant Inlet Temperature
	36	Engine Coolant Outlet Temperature
	37	Test Room Air Temperature
	38	Air Filter Temperature
	39	Crankcase Relative Pressure
GT-SUITE variables	40	In-Cylinder Trapped O2 Mass
	41	MFB10
	42	MFB50
	43	MFB75
	44	MFB90
	45	Burned gas temperature at MFB50
	46	Burned gas temperature at MFB75
	47	Burned Gas Temperature at MFB90
	48	Exhaust Manifold Temperature
	49	EGR Rate
	50	In-Cylinder Residual Gas Fraction
	51	Swirl Number at Start of Pilot 2 Injection
	52	Swirl Number at Start of Pilot 1 Injection
	53	Swirl Number at Start of Main Injection
	54	Swirl Number at Start of Combustion
	55	Swirl Number at MFB50
	56	Swirl number at MFB75
	57	Swirl number at MFB90
	58	Liquid Fuel Penetration Length at Start of Pilot 2 Injection
	59	Liquid Fuel Penetration Length at Start of Pilot 1 Injection
	60	Liquid Fuel Penetration Length at Start of Main Injection
	61	Diesel Fuel Concentration at Start of Combustion
	62	Maximum Spray Unburned Zone Volume

the work reported in this paper.

Data availability

The data that has been used is confidential.

Appendix

Table A1, Table A2

References

[1] ACEA Proposal for Euro 7, (June), 2021.

[2] ACEA Proposal for Euro VII, (June), 2021.

[3] A. Lefebvre, S. Guilain, Study of different boosting technologies and their effect on the transient response of a very downsized Diesel engine. SIA Congrès Le diesel: aujourd'hui et demain, 2012.

[4] T. Schnorbus, J. Schaub, M. Miccio, F. Glados, et al., Mild Hybridisation and Electric Boosting Improving Diesel Emissionsand Fuel Efficiency with Premium Performance, Aachener Kolloquium, 2015.

[5] A. Piano, F. Millo, D. Di Nunno, A. Gallone, Numerical analysis on the potential of different variable valve actuation strategies on a light duty diesel engine for improving exhaust system warm up, SAE Technical Paper 2017-24-0024 (2017), https://doi.org/10.4271/2017-24-0024.

[6] A. Piano, F. Millo, D. Di Nunno, A. Gallone, Numerical assessment of the CO2 reduction potential of variable valve actuation on a light duty diesel engine, SAE Technical Paper 2018-37-0006, (2018), https://doi.org/10.4271/2018-37-0006.

[7] J. Hofstetter, P. Boucharel, F. Atzler, G. Wachtmeister, Fuel consumption and emission reduction for hybrid electric vehicles with electrically heated catalyst, SAE Int. J. Adv. & Curr. Prac. in Mobility 3 (1) (2021) 702–714, https://doi.org/10.4271/2020-37-0017.

[8] Karamitros, D., Avgerinos, C., Skarlis, S., Koltsakis, G. et al., "Model-based comparison of passive SCR aftertreatment systems for electrified diesel applications," SAE Technical Paper 2020-37-0023, 2020, 10.4271/2020-37-0023.

[9] J. Demuynck, C. Favre, D. Bosteels, G. Randlshofer, et al., Integrated diesel system achieving ultra-low urban and motorway NOx emissions on the road, in: Proceedings of the 40th International Vienna Motor Symposium, 2019.

[10] F. Ravet, Crucial needs for efficient simulations in automotive industry, in: Proceedings of the CONVERGE User Conference, 2019.

[11] Millo, F., Boccardo, G., Piano, A., Arnone, L. et al., "Numerical simulation of the combustion process of a high EGR, high injection pressure, heavy duty diesel engine," SAE Technical Paper 2017-24-0009, 2017, 10.4271/2017-24-0009.

[12] A. Onorati, G. Montenegro, 1D and multi-D modeling techniques for IC engine simulation, SAE (2020).

[13] F. Sapio, A. Piano, F. Millo, F. Pesce, Digital shaping and optimization of fuel injection pattern for a common rail automotive diesel engine through numerical simulation. SAE Technical Paper 2017-24-0025, 2017, https://doi.org/10.4271/2017-24-0025.

[14] A. Piano, F. Millo, F. Sapio, F. Pesce, Multi-objective optimization of fuel injection pattern for a light-duty diesel engine through numerical simulation, SAE Int. J. Engines 11 (6) (2018) 1093–1107, https://doi.org/10.4271/2018-01-1124.

[15] Mallamo, F., Badami, M., and Millo, F., "Application of the Design of Experiments and Objective Functions for the Optimization of Multiple Injection Strategies for Low Emissions in CR Diesel Engines," SAE Technical Paper 2004-01-0123, 2004, 10.4271/2004-01-0123.

[16] Castagne, M., Bentolila, Y., Halle, A., Nicolas, F., et al., "Engine calibration : towards an integrated approach," IAV conference - DOE in Engine Development, May 2007, Berlin, Germany.

[17] Sjoblom, J., Andric, J., and Faghani, E., "Intrinsic Design of Experiments for Modeling of Internal Combustion Engines," SAE Technical Paper 2018-01-1156, 2018, 10.4271/2018-01-1156.

[18] X. Yu, L. Zhu, Y. Wang, D. Filev, et al., Internal combustion engine calibration using optimization algorithms, Appl. Energy 305 (2022), 117894, https://doi.org/10.1016/j.apenergy.2021.117894.

[19] K. Röpke, W. Baumann, B.U. Köhler, S. Schaum, et al., Engine calibration using nonlinear dynamic modeling, Lect. Notes Control Inf. Sci. 418 (2012) 165–182, https://doi.org/10.1007/978-1-4471-2221-0_10.

[20] F. Bozza, V. De Bellis, L. Teodosio, A numerical procedure for the calibration of a turbocharged spark-ignition variable valve actuation engine at part load, Int. J. Engine Res. 18 (8) (2017) 810–823, https://doi.org/10.1177/1468087416674653.

[21] S. Grasreiner, J. Neumann, M. Wensing, C. Hasse, Model-based virtual engine calibration with the help of phenomenological methods for spark-ignited engines, Appl. Therm. Eng. 121 (190–199) (2017), https://doi.org/10.1016/j.applthermaleng.2017.04.046.

[22] A. Sediako, J. Andric, J. Sjoblom, E. Faghani, Heavy duty diesel engine modeling with layered artificial neural network structures, SAE Technical Paper 2018-01-0870 (2018), https://doi.org/10.4271/2018-01-0870.

[23] X.H. Fang, N. Papaioannou, F. Leach, M.H. Davy, On the application of artificial neural networks for the prediction of NOx emissions from a high-speed direct injection diesel engine, Int. J. Engine Res. (2020), https://doi.org/10.1177/1468087420929768.

[24] M. Mirzaeian, S. Langridge, Creating a virtual test bed using a dynamic engine model with integrated controls to support in-the-loop hardware and software optimization and calibration, Energies 14 (2021) 652, https://doi.org/10.3390/en14030652.

[25] S. Lee, P.J. Andert, V. Vka, C. Quérel, et al., Virtual calibration based on X-in-the-loop : HiL simulation of virtual diesel powertrain, Simulation und Test 2017 Proceedings (2017), https://doi.org/10.1007/978-3-658-20828-8_4.

[26] F. Zhao, W. Yang, W. Yu, A progress review of practical soot modelling development in diesel engine combustion, J. Traffic Transp. Eng. (English Ed.) 7 (3) (2020) 269–281, https://doi.org/10.1016/j.jtte.2020.04.002.

[27] A. Piano, F. Millo, G. Boccardo, M. Rafigh, et al., Assessment of the predictive capabilities of a combustion model for a modern common rail automotive diesel engine. SAE Technical Paper 2016-01-0547, 2016, https://doi.org/10.4271/2016-01-0547.

[28] F. Millo, A. Piano, B. Peiretti Paradisi, M.R. Marzano, et al., Development and assessment of an integrated 1D-3D CFD codes coupling methodology for diesel engine combustion simulation and optimization, Energies 13 (7) (2020), https://doi.org/10.3390/en13071612.

[29] Y. He, C.J. Rutland, Application of artificial neural networks in engine modelling, Int. J. Engine Res. 5 (4) (2004) 281–296, https://doi.org/10.1243/146808704323224204.

[30] J.M. Alonso, F. Alvarruiz, J.M. Desantes, L. Hernández, et al., Combining neural networks and genetic algorithms to predict and reduce diesel engine emissions, IEEE Trans. Evol. Comput. 11 (1) (2007) 46–55, https://doi.org/10.1109/TEVC.2006.876364.

[31] S. Uslu, M.B. Celik, Prediction of engine emissions and performance with artificial neural networks in a single cylinder diesel engine using diethyl ether, Eng. Sci. Technol. an Int. J. 21 (6) (2018) 1194–1201, https://doi.org/10.1016/j.jestch.2018.08.017.

[32] F. Millo, A. Piano, A. Zanelli, G. Boccardo, et al., Development of a fully physical vehicle model for off-line powertrain optimization: a virtual approach to engine calibration, SAE Technical Paper 2021-24-0004 (2021), https://doi.org/10.4271/2021-24-0004.

[33] S. Caputo, F. Millo, G. Boccardo, A. Piano, et al., Numerical and experimental investigation of a piston thermal barrier coating for an automotive diesel engine application, Appl. Therm. Eng. 162 (2019), https://doi.org/10.1016/j.applthermaleng.2019.114233.

[34] G. Boccardo, F. Millo, A. Piano, L. Arnone, et al., Experimental investigation on a 3000 bar fuel injection system for a SCR-free non-road diesel engine, Fuel 243 (2019), https://doi.org/10.1016/j.fuel.2019.01.122.

[35] J.-H. Lee, Y.-D. Ko, I.-G. Yun, K.-H. Han, Comparison of latin hypercube sampling and simple random sampling applied to neural network modeling of HfO 2 thin film fabrication, Trans. Electr. Electron. Mater. 7 (4) (2006) 210–214, https://doi.org/10.4313/teem.2006.7.4.210.

[36] G. Boccardo, E. Servetto, A. Seebooa, G. Sammut, et al., Development of a real time GT-POWER xRT model for virtual calibration, GLOBAL GT CONFERENCE (2020).

[37] Pinamonti, S., Brancale, D., Meister, G., and Mendoza, P., "A Correlation Methodology between AVL Mean Value Engine Model and Measurements with Concept Analysis of Mean Value Representation for Engine Transient Tests," SAE Technical Paper 2017-24-0053, 2017, 10.4271/2017-24-0053.

[38] Andric, J., Schimmel, D., and Heide, J., "Calibration Procedure for Measurement-Based Fast Running Model for Hardware-in-the-Loop Powertrain Systems," SAE Technical Paper 2020-01-0254, 2020, 10.4271/2020-01-0254.

[39] Gamma Technologies, "GT-SUITE Engine Performance Application Manual", 2021.

[40] Russell, M., "Diesel Engine Noise: Control at Source," SAE Technical Paper 820238, 1982, 10.4271/820238.

[41] AVL, "Operative Instructions AVL 450 Combustion Noise Meter," 1986.

[42] F. Millo, A. Zanelli, L. Rolando, R. Fuso, Development of a comprehensive model for the concurrent minimization of CO2 and NOx emissions of a 48 V mild-hybrid diesel car, SAE Int. J. Elec. Veh. 10 (2) (2021) 177–194, https://doi.org/10.4271/14-10-02-0014.

[43] K. Witz, D.E. Hinkle, W. Wiersma, S.G. Jurs, Applied statistics for the behavioral sciences, J. Educ. Stat. 15 (1) (1990) 84, https://doi.org/10.2307/1164825.

[44] M. Kuhn, K. Johnson, Applied Predictive Modeling, Springer, 2013, https://doi.org/10.1007/978-1-4614-6849-3.

[45] K. Hornik, M. Stinchcombe, H. White, Multilayer feedforward networks are universal approximators, Neural Networks 2 (5) (1989) 359–366, https://doi.org/10.1016/0893-6080(89)90020-8.

[46] Heaton, J., "Ian Goodfellow, Yoshua Bengio, and Aaron Courville: Deep learning," *Genet. Program. Evolvable Mach.* 19(1–2):305–307, 2018, 10.1007/s10710-017-9314-z.

[47] X. Glorot, Y. Bengio, Understanding the difficulty of training deep feedforward neural networks, in: Proceedings of the Thirteenth International Conference on Artificial Intelligence and Statistics, 2010, pp. 249–256.

[48] S. Arlot, A. Celisse, A survey of cross-validation procedures for model selection, Stat. Surv. 4 (2010), https://doi.org/10.1214/09-SS054.